Cell, Vol. 93, 639–648, May 15, 1998, Copyright ©1998 by Cell Press

Molecular Basis of Lysosomal Enzyme Recognition: Three-Dimensional Structure of the Cation-Dependent Mannose 6-Phosphate Receptor

David L. Roberts, Daniel J. Weix, Nancy M. Dahms,* and Jung-Ja P. Kim*
Department of Biochemistry
Medical College of Wisconsin
Milwaukee, Wisconsin 53226

Summary

Targeting of newly synthesized lysosomal hydrolases to the lysosome is mediated by the cation-dependent mannose 6-phosphate receptor (CD-MPR) and the insulin-like growth factor II/cation-independent mannose 6-phosphate receptor (IGF-II/CI-MPR). The two receptors, which share sequence similarities, constitute the P-type family of animal lectins. We now report the three-dimensional structure of a glycosylation-deficient, yet fully functional form of the extracytoplasmic domain of the bovine CD-MPR (residues 3–154) complexed with mannose 6-phosphate at 1.8 Å resolution. The extracytoplasmic domain of the CD-MPR crystallizes as a dimer, and each monomer folds into a nine-stranded flattened β barrel, which bears a striking resemblance to avidin. The distance of 40 Å between the two ligand-binding sites of the dimer provides a structural basis for the observed differences in binding affinity exhibited by the CD-MPR toward various lysosomal enzymes.

Introduction

In higher eukaryotic cells, mannose 6-phosphate receptors (MPRs) mediate the delivery of newly synthesized soluble acid hydrolases to the lysosome by binding specifically to mannose 6-phosphate (Man-6-P) residues found on their N-linked oligosaccharides. The resulting MPR/lysosomal enzyme complex is transported from the Golgi to an acidified, prelysosomal compartment where the low pH of the compartment induces the complex to dissociate. The released lysosomal enzymes are packaged into lysosomes while the receptors either return to the Golgi to repeat the process or move to the plasma membrane where they function to internalize exogenous ligands. The observation that a defect in this targeting pathway results in a severe human lysosomal storage disease, mucolipidosis II, emphasizes the essential role of this phosphomannosyl recognition system in the biogenesis of lysosomes (for reviews, see von Figura and Hasilik, 1986; Dahms et al., 1989; Neufeld, 1991; Munier-Lehmann et al., 1996a).

Two distinct type I integral membrane glycoproteins have been identified as MPRs. The 46 kDa cation-dependent MPR (CD-MPR) exhibits optimum Man-6-P binding in the presence of divalent cations (Tong and Kornfeld, 1989; Li et al., 1990). Sequence analysis of the bovine CD-MPR reveals that it is comprised of a 28-residue amino-terminal signal sequence, a 159-residue extracytoplasmic domain, a single 25-residue transmembrane region, and a 67-residue carboxyl-terminal cytoplasmic domain (Dahms et al., 1987; see Figure 1). The second MPR, the 275 kDa insulin-like growth factor II/cation-independent MPR (IGF-II/CI-MPR), is multifunctional in that it binds proteins bearing the Man-6-P recognition marker as well as the peptide hormone IGF-II (Tong et al., 1988; Waheed et al., 1988; Kornfeld, 1992). The IGF-II/CI-MPR consists of an amino-terminal signal sequence, a 2269 residue extracytoplasmic region composed of 15 homologous repeating domains, a single transmembrane region, and a 163-residue carboxyl-terminal cytoplasmic domain. The extracytoplasmic region of the CD-MPR, unlike the transmembrane and cytosolic regions, shares sequence similarities (ranging from 14%–28% sequence identity) with each of the 15 repeating domains of the IGF-II/CI-MPR (Lobel et al., 1988). However, since these two receptors share no obvious sequence similarity with other lectins, it has been proposed that the two MPRs contain a distinct class of sugar-binding domains, resulting in their designation as P-type lectins (Drickamer and Taylor, 1993). Due to their common function in targeting lysosomal enzymes and the similarities in their amino acid sequence, it has been suggested that the MPRs evolved from a common ancestral gene (Dahms et al., 1987).

Little is known about the molecular interactions required for the specific binding of lysosomal enzymes by the MPRs. Equilibrium dialysis studies revealed that the CD-MPR binds 1 mol while the IGF-II/CI-MPR binds 2 mol of Man-6-P per polypeptide chain (Tong and Kornfeld, 1989; Tong et al., 1989). Therefore, the observation that the CD-MPR exists primarily as a dimer in membranes (Dahms and Kornfeld, 1989; Li et al., 1990; Punnonen et al., 1996) agrees with the hypothesis that two functional Man-6-P binding domains are needed for optimal lysosomal enzyme recognition. The two MPRs bind phosphomannosyl residues optimally in the pH range of 6.3–6.5, and no detectable binding is observed below pH 5, which is consistent with their ability to release lysosomal enzymes in the acidic environment of the prelysosomal compartment (Tong and Kornfeld, 1989). However, only the IGF-II/CI-MPR can bind ligand at neutral pH, which may explain why the CD-MPR cannot internalize ligands at the cell surface (Hoflack et al., 1987; Ma et al., 1991). The extracytoplasmic domain alone has been shown to be sufficient for Man-6-P binding by the CD-MPR (Dahms and Kornfeld, 1989; Wendland et al., 1989). His-105 and Arg-111 of the CD-MPR have been implicated in Man-6-P binding by chemical modification (Stein et al., 1987) and site-directed mutagenesis (Wendland et al., 1991a) studies. Additional studies have localized the two Man-6-P binding sites to domains 1–3 and 7–9 of the IGF-II/CI-MPR (Westlund et al., 1991; Dahms et al., 1993) and have identified Arg-435 in domain 3 and Arg-1334 in domain 9 as being essential components for phosphomannosyl recognition (Dahms et al., 1993). Sequence analyses revealed that Arg-111 of the CD-MPR is conserved in domain 3

*To whom correspondence should be addressed.

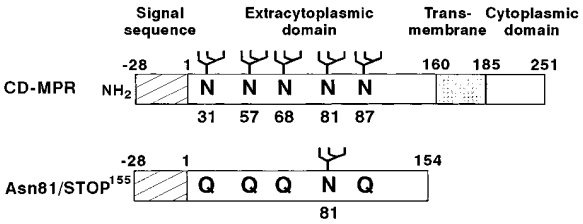

Figure 1. Schematic Presentation of Wild-Type and Mutant Bovine CD-MPR

The positions of the five potential N-linked glycosylation sites are indicated by the asparagine residues (N). The glycosylation-deficient mutant Asn-81/STOP^{155} was generated by replacing the proline (residue 155) codon in the bovine CD-MPR sequence (CCA, nucleotides 584–586) with a stop codon (TGA), thereby generating a protein lacking the transmembrane and cytoplasmic domains. In addition, four out of the five potential N-linked glycosylation sites were removed by replacing the asparagine residues at positions 31, 57, 68, and 87 with glutamine (Q) (Zhang and Dahms, 1993). Expression of the Asn-81/STOP^{155} construct in baculovirus-infected insect cells results in a secreted protein of 154 residues, and N-terminal sequencing demonstrated that the 28-residue N-terminal signal sequence (hatched box) has been removed.

(Arg-435) and domain 9 (Arg-1334) of the IGF-II/CI-MPR, suggesting that structural similarities exist between the ligand-binding sites of the two receptors.

To obtain insight into the mechanism by which these receptors bind lysosomal enzymes with high affinity, we have crystallized the extracytoplasmic domain of the CD-MPR in the presence of Man-6-P and have determined its three-dimensional structure at 1.8 Å resolution by the multiple isomorphous replacement method. The structure of the CD-MPR surprisingly exhibits striking similarities to the biotin binding protein avidin. The crystal structure reveals the nature of carbohydrate recognition by the CD-MPR and suggests a mechanism for the enhancement of ligand binding in the presence of divalent metals. Furthermore, we have modeled a complex between the receptor and a lysosomal enzyme, β-glucuronidase, which indicates that two separate oligosaccharide chains of a lysosomal enzyme must interact with the CD-MPR.

Results and Discussion

Expression of Recombinant Bovine CD-MPR

A truncated form of the bovine CD-MPR (Asn-81/STOP^{155}), consisting of the ligand-binding extracytoplasmic domain that has been modified to contain only a single N-glycosylation site, was generated (Figure 1). This glycosylation-deficient soluble form of the CD-MPR has been shown previously to exhibit ligand binding properties similar to those of the wild-type receptor (Zhang and Dahms, 1993). Asn-81/STOP^{155} was purified to apparent homogeneity by pentamannosyl phosphate-agarose affinity chromatography from the medium of baculovirus-infected *Trichoplusia ni* 5B1–4 (High Five) insect cells. Enzymatic deglycosylation of the purified protein demonstrated that it contained a single N-linked oligosaccharide. In addition, amino acid sequence analysis demonstrated that the 28-residue signal sequence was removed, as the N terminus (TEEKTXDLVGEK) was identical to that of the mature CD-MPR isolated from mammalian cells (Stein et al., 1987; N. M. D., unpublished data).

Table 1. Data Collection and Phasing Statistics

Diffraction Data	Native	K_2PtCl_4	K_2OsCl_6
Parameter			
Resolution (Å)	1.8	2.6	2.5
R_{merge}[a] (%)	7.7	7.9	7.4
Total observations	144,591	44,152	44,924
Unique reflections	31,187	10,270	12,190
Completeness (%)	89.0	85.8	90.8
MIRAS Phasing		K_2PtCl_4 (Pt_{ano})[b]	K_2OsCl_6
Parameter			
R_{iso}[c] (F)		11.1	7.0
(R_{ano})[d]		3.9	
Figure of merit[e]		0.667 (0.358)	0.599
Phasing power[f]		2.17 (1.79)	1.52
R_{cullin}[g]		0.533	0.607
Concentration (mM)		5	5
Soaking time (hr)		2	18
Number of sites		4	3
Final Model Statistics			
Final R factor[h]	22.1%		
R_{free}	26.1%		
rmsd bond lengths	0.006 Å		
rmsd bond angles	1.28°		
# of nonhydrogen atoms excluding water molecules	2621		
# water molecules	194		
Average B Factors (Å^2)			
Main chain	18.6		
Side chain	21.5		
Man-6-P	22.1		
Water	30.8		

The abbreviations are as follows: rmsd, root mean square deviation; MIRAS, multiple isomorphous replacement anomalous scattering.

[a] $R_{merge} = \Sigma_h\Sigma_i|I_{hi} - <I_h>|/\Sigma_h\Sigma_i|I_{hi}|$, where h indicates unique reflection indices and i indicates symmetry equivalent indices.

[b] Statistics for anomalous data sets are shown in parentheses.

[c] $R_{iso} = \Sigma||F_{ph}| - |F_p||/\Sigma|F_p|$ for isomorphous replacement (iso) data.

[d] $R_{ano} = \Sigma||F^+| - |F^-||/\Sigma|F^+|$ for acentric anomalous scattering (ano) data.

[e] The overall figure of merit was 0.561.

[f] Phasing power $= f_{rms}/E_{rms}$, where $f_{rms} = [(\Sigma f_H^2)/n]^{1/2}$ and $E_{rms} = [\Sigma(F_{PH} - |F_P + f_H|)^2/n]^{1/2}$.

[g] $R_{cullis} = \Sigma_h (|F_{PH} - F_P| - |f_H|)/\Sigma_H |F_{PH} - F_P|$ for all centric data.

[h] Reflections in the resolution range between 10 Å and 1.8 Å ($I > 2.0\ \sigma$) were used for refinement. Approximately 10% (3138 reflections) of the total reflections was used for R_{free} calculations.

Description of the CD-MPR Polypeptide Fold

The three-dimensional structure of the CD-MPR was determined to 1.8 Å resolution (R factor = 22.1% and free R factor = 26.1%). Data collection, phase determination, and refinement statistics are summarized in Table 1. The CD-MPR folds into a distinct, compact domain as shown in Figure 2B. Beginning with Glu-3, which is the third residue in the mature protein, the electron density is continuous through Ser-154, with the exception of the loop containing residues Val-38–Asp-43 (VGQSPD), which shows no observable electron density. Although the entire oligosaccharide chain of this glycosylated protein is not visible, a single N-acetylglucosamine residue, which is attached to Asn-81, is clearly discernable.

The CD-MPR consists almost entirely of β strands,

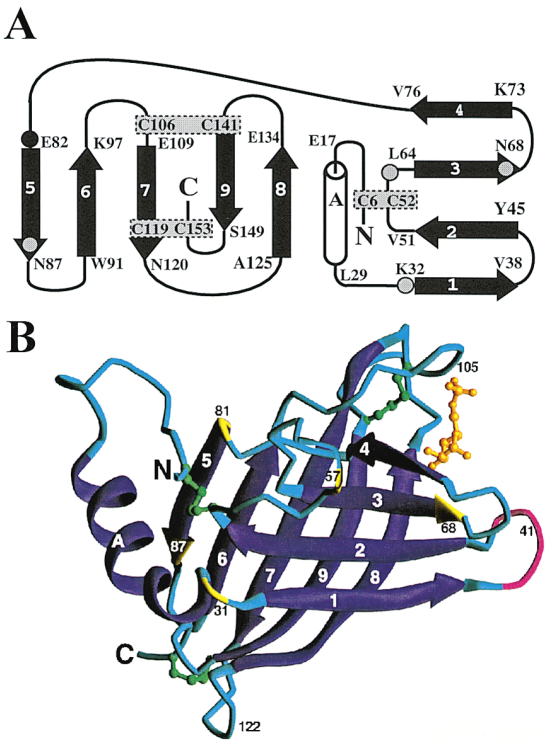

Figure 2. The CD-MPR Is Composed Primarily of β Strands

(A) Topology of the bovine CD-MPR structure. β strands are represented by black arrows, while the α helix is indicated by a cylinder. Disulfide bonds are enclosed by shaded, dashed boxes. Light gray circles represent the four N-linked glycosylation sites that have been removed by the substitution of Asn residues with Gln residues. The closed, black circle represents the single intact glycosylation site at position 81. Numbering of residues is based on the mature protein sequence. The β strands are numbered from N to C terminus, beginning with 1, while the α helix is labeled as "A." The residue located at the beginning and end of each secondary structural element is indicated.

(B) Ribbon diagram of the bovine CD-MPR structure. Disulfide bonds are indicated (green ball-and-stick model). The locations of the five potential N-glycosylation sites are also highlighted (yellow ribbons). However, in the Asn-81/STOP[155] glycosylation-deficient mutant, only the asparagine residue at position 81 is glycosylated. The density is continuous throughout the entire molecule with the exception of the loop between strands 1 and 2 (pink ribbon). The location of Man-6-P is shown (gold ball-and-stick model).

with only one α helix located at the N-terminal region of the molecule (Figure 2). The β strands form two β sheets that are positioned orthogonal to one another, giving rise to a flattened β barrel arrangement. Following the N-terminal α helix, the molecule contains a four-stranded, antiparallel β sheet, extending from Lys-32 through Val-76. The molecule then extends through five more β strands, forming the second β sheet. The antiparallel strands are sequentially connected throughout the molecule, with the exception of the last two β strands, which switch places in order to form a necessary disulfide bond. All six cysteine residues of the extracytoplasmic domain of the CD-MPR are involved in disulfide bond formation. Since each of the three disulfide bonds (Cys-6–Cys-52, Cys-106–Cys-141, and Cys-119–Cys-153) are located within a β sheet, they do not participate in connecting one β sheet to the other. This disulfide bonding pattern was previously predicted for the CD-MPR based on amino acid alignments between the CD-MPR and each of the 15 repeating domains of the IGF-II/CI-MPR (Lobel et al., 1988) and on subsequent mutational studies (Wendland et al., 1991b). The interactions between the two β sheets of the CD-MPR are primarily hydrophobic in nature. The residues involved in association of the two β sheets consist of Leu-29, Phe-34, Phe-49, Val-51, Leu-64, Val-77, Ile-92, Leu-94, Ala-113, Val-115, Ile-117, Phe-128, Phe-145, Met-147, and Leu-151 (see Figure 6). These residues form a hydrophobic core that collapses the interior of the CD-MPR protein, thus making the overall structure very tight and compact.

Comparison of the CD-MPR to Other Known Protein Structures

In an attempt to identify other proteins that have a fold similar to the CD-MPR, two methods were used. First, the structures of all the known lectins, which are indexed at http://www.cermav.cnrs.fr/databank/lectine/, were compared one at a time to the CD-MPR coordinates using the program "FIT" (distributed from http://gamma.mbb.ki.se/~guoguang/fit.html). The superimposed structures were then manually inspected to determine whether structural similarities exist. Second, the coordinates for the CD-MPR were submitted to the DALI server (http://www2.ebi.ac.uk/dali/), which performs a three-dimensional structure comparison of the query structure to a representative set of the entire pdb database (Holm and Sander, 1993). These analyses confirmed that the CD-MPR bears no resemblance to other lectins for which structural information is available. However, the CD-MPR was found to exhibit a fold topologically similar to that of avidin, a protein with which it exhibits less than 10% sequence similarity, with a root mean square (rms) deviation of only 1.9 Å among main-chain atoms of 78 residues that form the two β sheets, excluding variable loop regions. Figure 3 shows a comparison of the CD-MPR and avidin polypeptide folds. What is striking about this finding is that not only are the CD-MPR and avidin topologically similar (identical through strand 7, then strands 8 and 9 of the CD-MPR are reversed from that of the avidin fold), but the almost orthogonal arrangement that is observed between the two β sheets of the CD-MPR, forming the flattened β barrel structure, is also conserved. Both proteins bind to their ligand at a similar location in the structure. However, in comparison to the Man-6-P binding site in the CD-MPR, the biotin binding site is positioned deeper within the avidin molecule. Based on the similarities between the two structures, it is intriguing to speculate that the CD-MPR utilizes the same polypeptide fold as avidin in order to facilitate high-affinity ligand binding.

The CD-MPR Is a Dimer

Crystals of the CD-MPR reveal the presence of two molecules of the CD-MPR per asymmetric unit. The spatial arrangement of these molecules is shown in Figure 4A. The rms deviation between the main-chain atoms of the two monomers is 0.10 Å, demonstrating that their structures are identical. In addition, both monomers show no observable electron density for residues 38–43, suggesting that this region is very dynamic in the native

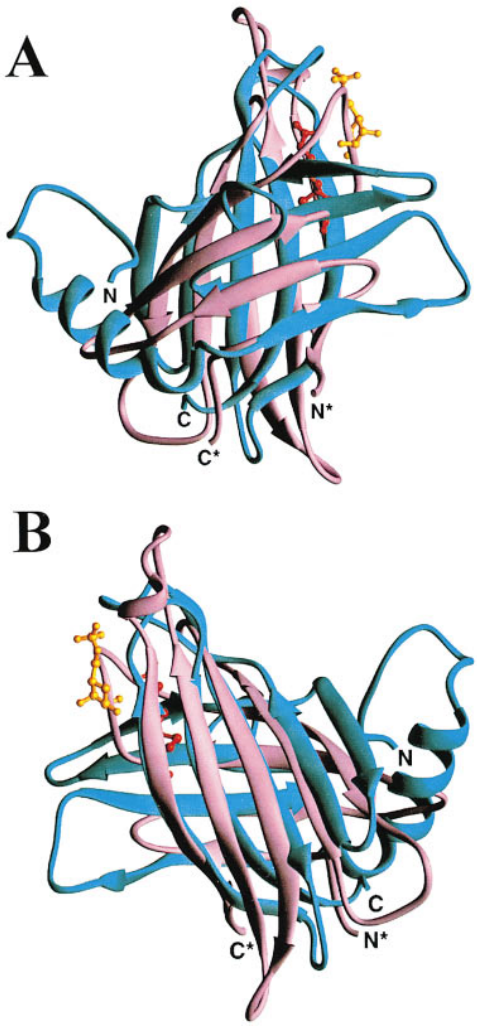

Figure 3. Similarity between the CD-MPR and Avidin Folds

(A and B) The CD-MPR structure (cyan ribbon) was overlapped with that of avidin (magenta ribbon; PDB accession code 1AVE) using DALI. The rms deviation between main-chain atoms (excluding variable loop regions) is 1.9 Å. The ligand-binding sites are located topologically in similar positions on the two molecules (red ball-and-stick model for avidin; gold ball-and-stick model for Man-6-P). The N and C termini of the CD-MPR are labeled, as are the N* and C* termini of avidin. The two views are oriented 180° to each other.

structure. As is seen with the interactions between the β sheets of one monomer, the interactions between the two monomers are primarily hydrophobic in nature (Figure 4B), including residues Val-9, Gly-10, Phe-86, Trp-91, Met-93, Ile-95, Val-114, Met-116, Val-131, Val-138, Phe-142, and Leu-144. The contact surface area between the two monomers of the dimer is 1550 $Å^2$ per monomer, which is approximately 20% of the entire surface area of one CD-MPR monomer (8231 $Å^2$). Since this is the most hydrophobic surface of the CD-MPR and, in general, such a large hydrophobic surface would not be solvent exposed, this crystallographic dimer most likely represents the functional form of the CD-MPR. These structural data support previous biochemical studies which indicate that the CD-MPR exists predominantly as a dimer in membranes (Dahms and Kornfeld, 1989; Li et al., 1990; Punnonen et al., 1996).

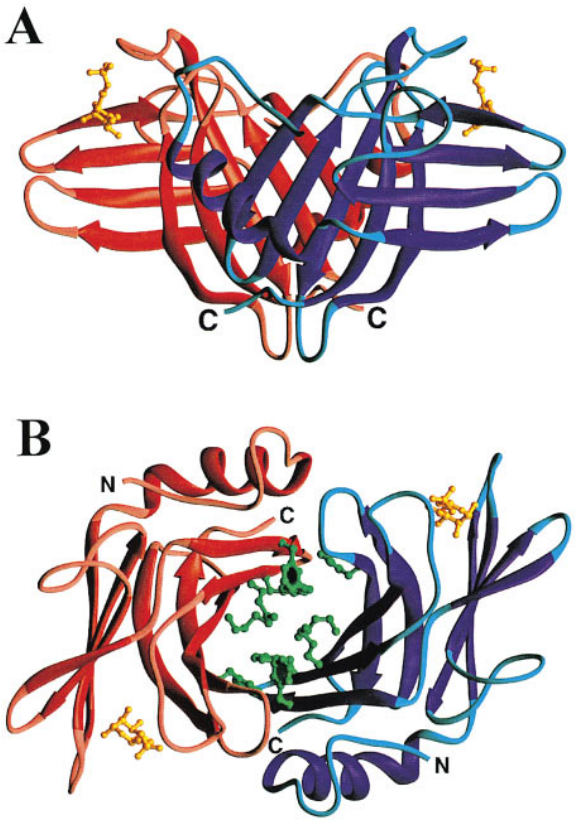

Figure 4. The CD-MPR Exists as a Dimer

(A) Ribbon diagram of the bovine CD-MPR dimer. There are two CD-MPR monomers (red/rose ribbon and blue/cyan ribbon) within the asymmetric unit. These monomers are related by a noncrystallographic 2-fold axis parallel to the YZ plane (45° off the x axis). The ligand, Man-6-P, is also shown (gold ball-and-stick model).

(B) The interactions at the dimer interface are primarily hydrophobic in nature. Residues forming the interface between the two monomers are shown (green ball-and-stick model). This view is looking from the "top" of that shown in (A).

The Structure Reveals the Nature of Carbohydrate Recognition by the CD-MPR

The crystals of the CD-MPR were obtained in the presence of Man-6-P and the divalent cation, Mn^{+2}. Both $|2F_o - F_c|$ and $|F_o - F_c|$ difference Fourier maps yielded well-defined electron density (Figure 5A) located at the end of the β barrel (Figures 2B and 4A). Each monomer is complexed with a single Man-6-P molecule (Figures 2B and 4A), which is consistent with previous Scatchard analyses that determined a stoichiometry of ligand binding of one Man-6-P molecule per CD-MPR monomer (Tong and Kornfeld, 1989) and with the observation that a monomeric form of the receptor can bind ligand (Dahms and Kornfeld, 1989). Residues found in loop regions as well as in β strands from both β sheets are involved in binding ligand (Figures 5B and 6). Studies which showed that a complete loss of binding activity occurs following either the reduction of the CD-MPR with dithiothreitol (Li et al., 1990) or the replacement of each of the six Cys residues with Gly (Wendland et al., 1991b) have indicated the importance of disulfide linkages in carbohydrate recognition. Analysis of the structure confirms that disulfide bond formation is important in the stabilization and/or orientation of the loop

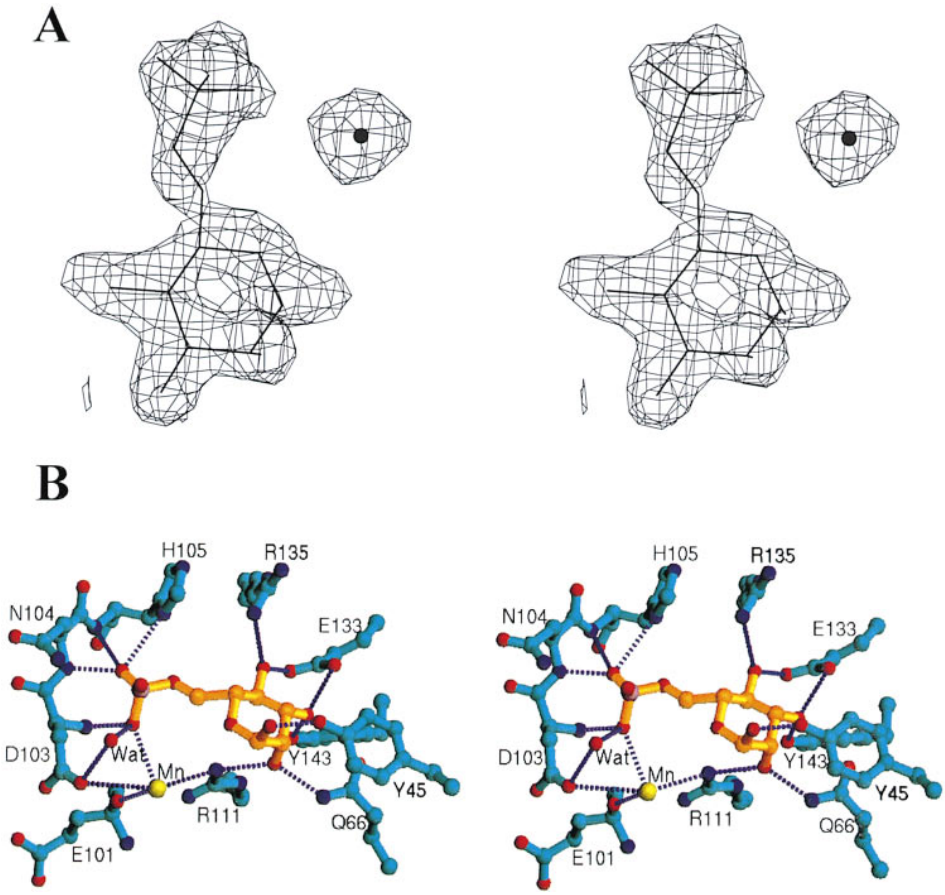

Figure 5. The CD-MPR Contains Bound Man-6-P

(A) Stereo diagram of a model of Man-6-P fitted into the final electron density map. A $|2F_o - F_c|$ difference Fourier map was calculated at 1.8 Å and contoured at 1.2 σ. The $|2F_o - F_c|$ density is also shown for the Mn^{+2} ion (dark circle).

(B) Stereo view of the complex network of hydrogen bonds formed between Man-6-P and residues in the binding site region of the CD-MPR. Residues within the ligand-binding site are shown (cyan ball-and-stick model), along with Man-6-P (gold ball-and-stick model). Potential hydrogen bonds are indicated by blue dotted lines. Atoms are colored as follows: red, oxygen atoms; blue, nitrogen atoms; cyan, protein carbon atoms; gold, ligand carbon atoms; yellow, Mn^{+2}; lavender, phosphate atom; Wat, water molecule (red sphere).

involved in Man-6-P binding (Figure 2B). The disulfide bond between Cys-106 and Cys-141 appears to be of particular importance, as it brings two loops (loop between β strands 6 and 7, and loop between β strands 8 and 9) together to form the Man-6-P binding cavity.

Two residues that were previously mutated and shown to be important for Man-6-P recognition (Wendland et al., 1991a), His-105 and Arg-111, are located within the ligand-binding site (Figure 5B). His-105 functions in binding the negatively charged phosphate group of the

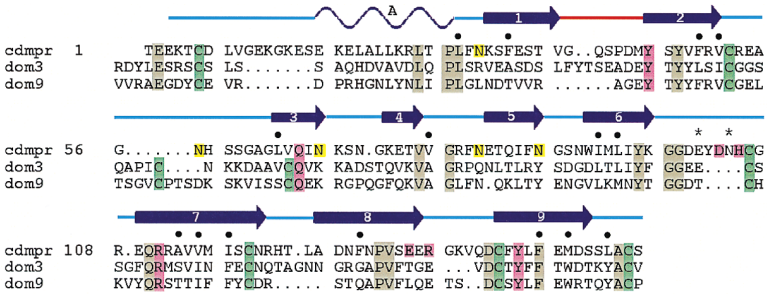

Figure 6. Comparison of the CD-MPR with Domains 3 and 9 of the IGF-II/CI-MPR

The sequence alignment was generated using the BESTFIT algorithm (Genetics Computer Group program, University of Wisconsin-Madison). The output was modified such that gaps and insertions were placed in variable loop regions. The secondary structure of the CD-MPR is shown above the sequence. The arrows designate β strands, and the wavy line represents the single α helix. Residues involved in Man-6-P binding are shown in pink. The five potential N-glycosylation sites are shown in yellow. Cysteine residues are shown in green. Residues that are conserved are shaded in gray. The numbering is based on the mature CD-MPR sequence. The small circles above the letters indicate the residues of the CD-MPR that are involved in the association of the two β sheets. The asterisk above E101 and N104 indicates that these residues participate in main-chain interactions with the Mn^{+2} and Man-6-P, respectively. The red line between strands 1 and 2 represents the disordered loop region as shown in Figure 2B. The wild-type CD-MPR sequence is shown and therefore contains Asn residues at positions 31, 57, 68, 81, and 87. However, the construct that was used to determine the structure contained Gln at each of these positions, with the exception of position 81 where the Asn was retained.

ligand. Of the residues located in the binding site, His-105 is the most likely candidate to confer the pH dependence that is observed in phosphomannosyl binding. Arg-111 is hydrogen bonded to the C2 oxygen atom of the mannose ring and, although not in close proximity for hydrogen bonding interactions with the phosphate oxygens (about 4.1 Å away), may also provide a positively charged environment for the phosphate moiety of the ligand. The main-chain atoms of Asp-103, Asn-104, and His-105, a water molecule that is hydrogen bonded to the carboxylate of Asp-103, and a Mn^{+2} complete the interactions involved in binding the phosphate portion of the sugar.

The CD-MPR was originally identified and purified based on its enhanced ligand binding ability in the presence of divalent cations, particularly Mn^{+2} (Hoflack and Kornfeld, 1985a, 1985b). Asp-103, which is located within the loop containing His-105 between strands 6 and 7, coordinates the Mn^{+2} cation. In addition, the carbonyl oxygen of Glu-101 and a guanidino nitrogen of Arg-111 coordinate the Mn^{+2} cation. The divalent cation in turn ligates one of the phosphate oxygen atoms of the Man-6-P ligand. In the absence of cations, it is predicted that Asp-103 could directly interact and form hydrogen bonds with the phosphate oxygen atoms, although charge interactions may interfere with ligand binding. These findings are consistent with previous biochemical studies which show that binding of the CD-MPR to a phosphomannosyl affinity column is inhibited in the presence of EDTA (Hoflack and Kornfeld, 1985b). In addition, equilibrium dialysis binding studies using the CD-MPR purified from bovine liver demonstrated a 4-fold increase in affinity for pentamannosyl phosphate in the presence of $MnCl_2$ (Tong and Kornfeld, 1989).

Residues involved in forming hydrogen bonds with the hydroxyl groups of mannose include Arg-135 (C4 hydroxyl), Glu-133 (C3 and C4 hydroxyls), Tyr-143 (C3 hydroxyl), Arg-111 (C2 hydroxyl), Gln-66 (C2 hydroxyl), and Tyr-45 (C1 hydroxyl). These residues, along with Asp-103, Asn-104, and His-105, are conserved among bovine, human, and murine CD-MPRs (Köster et al., 1991). In addition, site-directed mutagenesis studies have confirmed the essential nature of these residues for Man-6-P binding: CD-MPRs containing a single amino acid substitution at position 66, 105, 111, 133, 135, or 143 exhibit a dramatic loss in the ability to bind to a pentamannosyl phosphate-agarose affinity column (Wendland et al., 1991a; L. Olson and N. M. D., unpublished data). Inhibition studies using chemically synthesized oligomannosides or neoglycoproteins have demonstrated that the presence of the phosphomonoester Man-6-P at a terminal position is the major determinant for ligand recognition and that linear mannose sequences which contain a terminal Man-6-P linked α1,2 to the penultimate mannose are the most potent inhibitors (Distler et al., 1991). Additional studies using sugar analogs of Man-6-P have shown that the phosphate group and axial 2-hydroxyl moiety of Man-6-P are critical for ligand binding (Tong and Kornfeld, 1989), which is reflected in the number of interactions these moieties have with the protein (Figure 5B). In contrast to that observed for many of the mannose/glucose-specific binding lectins (Weis and Drickamer, 1996), the binding of Man-6-P to the CD-MPR does not require stacking interactions with aromatic side chains.

Tyr-45 is located at the beginning of strand 2, which is at the C-terminal end of the disordered loop region (Figure 2). In the structure, Tyr-45 shows very well-defined electron density and hydrogen bonds with the C1-hydroxyl of Man-6-P. Since the endogenous ligands of the CD-MPR are glycoproteins containing terminal phosphomannosyl residues on high mannose-type oligosaccharide chains, this hydroxyl group would be involved in a glycosidic linkage and thus would not be available for hydrogen bonding interactions. The location of Tyr-45 in a flexible portion of the molecule suggests that Tyr-45 could move to accommodate a bound oligosaccharide chain. In the apoavidin structure, a loop containing residues 36–44 is disordered but becomes ordered upon binding biotin (Livnah et al., 1993). This loop in the avidin structure is analogous to the loop preceding Tyr-45 of the CD-MPR (residues 38–43). Thus, this disordered loop in the CD-MPR may be flexible to allow ligand to bind, becoming ordered only in the presence of an oligosaccharide. The finding that electron density is observed for all residues in this loop in the crystal structure of the CD-MPR complexed with pentamannosyl phosphate supports this hypothesis (L. Olson, J. Zhang, N. M. D., and J.-J. P. K., unpublished data).

Previous studies have indicated that oligosaccharides containing Man-6-P residues in phosphodiester linkage with either N-acetylglucosamine or a methyl group bind poorly to the CD-MPR (Hoflack et al., 1987; Tong and Kornfeld, 1989; Distler et al., 1991). The configuration of the ligand-binding site of the CD-MPR is consistent with these biochemical studies. Approximately 65% of the Man-6-P surface is buried by the receptor, and particularly, the phosphate moiety is quite concealed, leaving no room in the structure to accommodate a phosphodiester.

As shown in Figure 4A, the two carbohydrate binding sites of the CD-MPR dimer are spaced widely apart and are oriented in the same direction. This parallel binding site arrangement is observed in several oligomeric lectins, such as ricin, the mannose binding protein, and cholera toxin (Drickamer, 1995). The linear distance between the two Man-6-P sites is approximately 40 Å, which is too great for a single high mannose-type oligosaccharide to span (a typical distance between the terminal mannose residues of a high mannose-type oligosaccharide is ≈20 Å). The structure is consistent with previous studies which showed that diphosphorylated oligosaccharides bound to the CD-MPR with an affinity similar to that of Man-6-P ($K_d = 2 \times 10^{-7}$ M versus 8×10^{-6} M) (Tong and Kornfeld, 1989; Tong et al., 1989). This is in contrast to that observed for the IGF-II/CI-MPR where a diphosphorylated oligosaccharide bound with an affinity similar to that of lysosomal enzymes ($K_d = 2 \times 10^{-9}$ M versus 1×10^{-9} M). However, in these studies, the stoichiometry of binding was determined to be 0.5 molecules of the diphosphorylated oligosaccharide per monomer of the CD-MPR, indicating that a single oligosaccharide can span the two binding sites of the dimer. One possible explanation may relate to the oligomeric state of the CD-MPR during the binding

studies. Chemical cross-linking studies have indicated that the CD-MPR exists as dimers and tetramers in detergent solution (Li et al., 1990; Waheed et al., 1990; Ma et al., 1992). Several studies (Li et al., 1990; Waheed et al., 1990) have shown that increasing the receptor protein concentration in detergent solutions results in the formation of increasing amounts of tetramers, with a receptor concentration of 19 μM yielding a high percentage (68%) of tetrameric species (Waheed et al., 1990). Therefore, the high concentrations of detergent-solubilized receptor used in the binding studies by Tong and Kornfeld may have resulted in a high percentage of the CD-MPR existing as a tetramer. It is possible that as a tetramer, two carbohydrate binding sites are situated within the appropriate distance for a single diphosphorylated oligosaccharide to span. Another possible explanation for this discrepancy is that a conformational change occurs upon binding an oligosaccharide, bringing the two binding sites of the dimer in close proximity to each other. However, for this to occur, the conformational change would have to be quite dramatic and thus represents a less likely mechanism.

Structure-Based Sequence Alignment of Domain 3 and Domain 9 of the IGF-II/CI-MPR

The extracytoplasmic region of the CD-MPR shares sequence similarities (ranging from 14%–28% sequence identity) with each of the 15 repeating domains of the IGF-II/CI-MPR (Lobel et al., 1988). Of the 15 repeating domains of the IGF-II/CI-MPR, only domains 3 and 9 have been shown to be essential for binding Man-6-P (Dahms et al., 1993). Therefore, we proceeded to model domains 3 and 9, using the structure of the CD-MPR as a template, in order to gain insight into the mechanism of carbohydrate recognition by the IGF-II/CI-MPR. A structure-based sequence alignment was generated between the CD-MPR and domains 3 and 9 of the IGF-II/CI-MPR by maintaining the positions of the cysteine residues involved in disulfide bond formation and placing gaps and insertions within the variable loop regions (Figure 6). Nonpolar residues involved in the association of the two β sheets in the CD-MPR (Figure 2) are also conserved in domains 3 and 9 (Figure 6), supporting the hypothesis that these domains of the IGF-II/CI-MPR form a similar polypeptide fold.

From the alignment, it is apparent that the loop regions in the vicinity of the carbohydrate binding site are altered in the IGF-II/CI-MPR. In domain 3 and domain 9, several of the residues that are responsible for ligand binding in the CD-MPR remain in place, including Tyr-45 (CD-MPR numbering), Gln-66, Arg-111, and Tyr-143. However, interactions with Glu-133 and Arg-135 have both been lost since these residues have been changed to Thr and Glu, respectively, in domain 3, and Leu and Glu, respectively, in domain 9 (Figure 6). Perhaps the largest difference between the ligand-binding sites exists in the loop containing residues 103–108. This loop, which connects strands 6 and 7 and is primarily responsible for binding and concealing the phosphate moiety of Man-6-P in the CD-MPR, is shorter by four residues (YDNH) in both domain 3 and domain 9 (Figure 6) and is predicted to result in the exposure of the phosphate moiety. These observations are consistent with previous binding studies, which show that the IGF-II/CI-MPR can bind oligosaccharides bearing phosphodiesters, containing either a methyl group or N-acetylglucosamine, while the CD-MPR cannot (Hoflack et al., 1987; Tong and Kornfeld, 1989; Distler et al., 1991). Neither domain 3 nor domain 9 contains a residue analogous to Asp-103, which coordinates the divalent cation and thus may explain why only the CD-MPR exhibits enhanced binding in the presence of divalent cations. Confirmation of the above models will have to await the structure of the IGF-II/CI-MPR.

Hypothetical Complex between the CD-MPR and β-Glucuronidase

In order to understand further the mechanism of ligand recognition by the CD-MPR, we have modeled the interaction of the CD-MPR with a lysosomal enzyme, β-glucuronidase (Protein Data Bank accession code 1BHG; Jain et al., 1996). In this model, we have oriented the CD-MPR with respect to the membrane such that the carbohydrate binding sites are situated at a distance from the membrane. Since the C-terminal Ser residue at position 154 is only five residues from the predicted transmembrane portion of the CD-MPR, it is likely that the two C termini of the dimer are in close proximity to the lipid bilayer. β-glucuronidase is a homotetrameric glycoprotein that has been shown to bind with high affinity to the CD-MPR (K_d = 0.28 nM, Watanabe et al., 1990; K_d = 4.4–5.1 nM, Ma et al., 1991). Each monomer of the human enzyme contains 651 residues, and all four of the potential N-linked glycosylation sites are glycosylated. However, only a single oligosaccharide chain, which is attached to Asn-173, is discernable in the crystal structure. Therefore, docking was performed by overlapping the terminal sugar of the oligosaccharide at position 173 in the β-glucuronidase structure with the Man-6-P of the CD-MPR structure (Figure 7). It is clear that the binding sites of the dimeric CD-MPR will readily accommodate the two oligosaccharide chains positioned on separate polypeptides chains of this tetrameric enzyme, but not a single diphosphorylated oligosaccharide. Although the oligosaccharide at position 173 may not be preferentially bound by the CD-MPR due to its relatively poor phosphorylation state in comparison to the oligosaccharides at the other three glycosylation sites (Shipley et al., 1993), the model does show how the CD-MPR could recognize two oligosaccharides located on different polypeptide chains of an oligomeric ligand and predicts that a similar type of mechanism could occur for phosphorylated oligosaccharides located on the same polypeptide. This model is consistent with recent studies which showed that the CD-MPR exhibits a higher affinity toward oligosaccharides with one phosphomonoester while the IGF-II/CI-MPR preferentially binds oligosaccharides containing two phosphomonoesters (Munier-Lehmann et al., 1996b). Thus, the differences in affinities exhibited by the CD-MPR toward different lysosomal enzymes (Sleat and Lobel, 1997) are likely to be due to the combined effects of the location and number of phosphomannosyl residues on the oligosaccharide and the spatial orientation of these sugar chains on the lysosomal enzyme molecule.

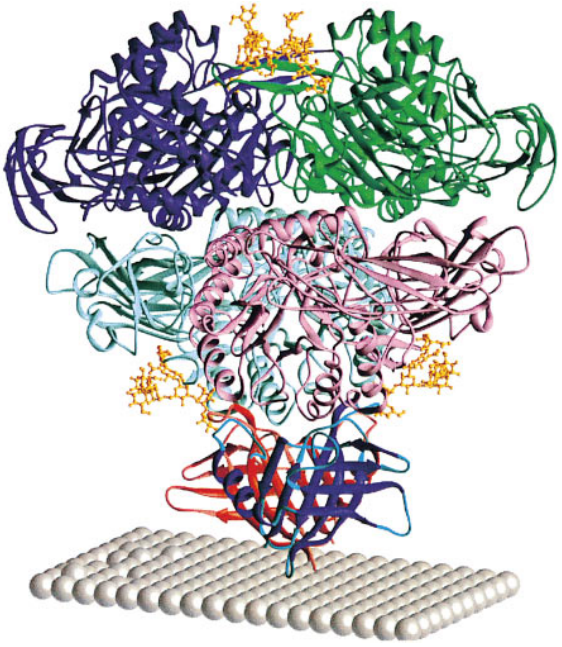

Figure 7. Molecular Modeling of a Complex between the CD-MPR and a Lysosomal Enzyme, β-Glucuronidase

The refined structure of the CD-MPR and the published coordinates of β-glucuronidase (PDB accession code 1BHG) were used. The CD-MPR dimer (blue/cyan and red/rose ribbons) are shown in the same orientation as in Figure 4A. The tetrameric β-glucuronidase protein is shown. The oligosaccharide attached to Asn-173 is also shown (gold ball-and-stick model). The model was generated by overlapping the terminal mannose residue of the β-glucuronidase oligosaccharide with the CD-MPR Man-6-P substrate. The location of the membrane is also indicated (gray spheres).

In summary, the structure of the extracytoplasmic domain of the CD-MPR reveals the mechanism of carbohydrate recognition by the P-type family of animal lectins and provides a model for lysosomal recognition by the MPRs. The information gained during these studies has led us to ask additional questions. For example, what is the molecular basis for the pH dependence of ligand binding and release by the MPRs? Is Asp-103 of the CD-MPR responsible for the enhancement of binding in the presence of divalent cation? Do the MPRs undergo a conformational change upon binding ligand? What is the nature of IGF-II binding to the IGF-II/CI-MPR, and is there any cooperativity between the IGF-II and carbohydrate binding sites of this receptor? Additional biochemical, biophysical, and structural studies will be required to answer these and other questions at the molecular level.

Experimental Procedures

Expression and Purification of Recombinant CD-MPR

A glycosylation-deficient form of the bovine CD-MPR containing the signal sequence and extracytoplasmic domain (Asn-81/STOP^{155}, Figure 1) was generated as described previously (Zhang and Dahms, 1993). The nonfusion AcNPV transfer vector pVL1393 (PharMingen) encoding the Asn-81/STOP^{155} construct (2 μg) and modified AcNPV baculovirus DNA (0.5 μg, BaculoGoldR DNA, PharMingen) were cotransfected into the *Spodoptera frugiperda* (Sf9) insect cell line, and recombinant virus was isolated as described previously (Dahms and Brzycki-Wessell, 1995). *Trichoplusia ni* 5B1–4 (High Five) insect cells were cultured in Express Five serum free medium (Life Technologies, Inc.) and maintained at 27°C. High Five cells in monolayer cultures were infected with the recombinant virus at a multiplicity of infection of 5–10 and the medium was harvested 4–5 days postinfection. Asn-81/STOP^{155} protein was purified from the medium to apparent homogeneity by pentamannosyl phosphate-agarose affinity chromatography as described previously (Dahms et al., 1993).

Crystallization and Data Collection

The purified CD-MPR was dialyzed against buffer (150 mM NaCl, 10 mM $MnCl_2$, 5 mM β glycerophosphate, and 10 mM Man-6-P in 50 mM imidazole [pH 6.5]) and concentrated to a final protein concentration of 8.8 mg/ml. Initial crystallization was performed by vapor diffusion using the hanging drop technique (McPherson, 1982) following the sparse matrix protocol (Carter and Carter, 1979). From the initial screening, four similar conditions resulted in crystal formation, with crystals ranging from needles to thin plates to thick rods. Modification of the initial conditions yielded diffraction quality crystals with dimensions of 0.2 mm × 0.2 mm × 0.8 mm. The final crystallization condition was obtained by mixing equal volumes of the concentrated protein (8.8 mg/ml in protein buffer) with precipitating solution (0.20 M ammonium acetate and 25% polyethyleneglycol 4000 in 0.10 M cacodylate buffer [pH 6.6]) and equilibrating against precipitating solution using the sitting drop vapor diffusion technique at 19°C.

A single crystal was mounted in a thin-walled glass capillary tube, and diffraction data were collected to 2.6 Å resolution at 4°C on an R-axis IIC image plate detector system with a Rigaku RU200 rotating anode generator operating at 50 kV and 100 mA with a graphite monochromator. Still photographs indicated that the crystal belonged to a tetragonal space group with unit cell parameters $a = b = 92.63$ Å and $c = 85.29$ Å. Assuming two molecules per asymmetric unit, the calculated Matthews' coefficient is 2.4 Å^3/Da (Matthews, 1968). Systematic absences at $h = \text{odd}$ for the h00 ($k = \text{odd}$ for the 0k0) reflections and at $l \neq 4n$ for the 00l reflections indicate that the CD-MPR crystals belong to either $P4_12_12$ or $P4_32_12$. One complete native data set was collected to 1.8 Å resolution, and the statistics of the collected data are shown in Table 1. The diffraction data were processed with the DENZO package (Otowinski and Minor, 1996).

Structure Determination and Refinement

The crystal structure of the CD-MPR was solved using multiple isomorphous replacement methods together with anomalous scattering data. Heavy atom screening was performed by soaking preformed crystals for various times in mother liquor containing various heavy atom compounds. Two isomorphous derivatives, K_2PtCl_4 and K_2OsCl_6, were used for initial phase determination. The positions of the heavy atoms were determined by inspection of difference Patterson maps and confirmed by difference Fourier techniques, using X-ray data with $I/\sigma > 3.0$, between 30 and 3.0 Å resolution. The positions and occupancies of the heavy atoms were first refined using the program HEAVY (Terwilliger, 1994), and multiple isomorphous replacement phases were calculated and refined using the PHASES package (Furey and Swaminathan, 1997). The assignment of the space group was made by calculating Fourier maps for both handedness for each space group using the Pt anomalous data. By comparing the quality of these maps, the space group was determined to be $P4_32_12$. Phasing statistics are given in Table 1. At this stage, the overall figure of merit was 0.561 for 11,267 reflections.

Initial electron density maps were calculated using data between 30 and 3.0 Å resolution, and the solvent flattening procedure (Wang, 1985) was used to improve the multiple isomorphous replacement phases. At this time, it was possible to locate the two molecules of the CD-MPR within the asymmetric unit and thus determine the position of the noncrystallographic 2-fold axis. Further density modification was carried out using noncrystallographic symmetry averaging as implemented in the PHASES package. An initial model was constructed using the molecular graphics program TURBO-FRODO (Roussel and Cambillau, 1994). At this stage, a polyalanine model was unambiguously constructed for the entire polypeptide chain, including the assignment of over 60% of the amino acid residues. Approximately 135 of the 154 total residues were built into the initial

model of the CD-MPR protein. Electron density maps were then generated by combining the multiple isomorphous replacement phases and those of the model according to the SIGMAA algorithm (Read, 1986). Phase combination allowed for the completion of the chain tracing, along with identification of the remaining amino acid residues and also identified that an incorrect tracing had been made through a disulfide bond. Correction of this tracing made it possible to complete the model building of the CD-MPR, including the total assignment of all the amino acid residues. The connectivity was confirmed using simulated annealing omit maps. Refinement of the structure was carried out using iterative cycles of X-PLOR energy minimization (Brünger, 1992) followed by manual fitting and rebuilding on a Silicon Graphics workstation using TURBO-FRODO graphics software. The two monomers in the asymmetric unit were refined using noncrystallographic symmetry (NCS) restraints until the R factor was approximately 28%, at which stage the NCS restraints were totally released. Ramachandran plot analysis indicates that over 85% of the residues reside in the most favored regions while none are observed in disallowed regions.

After each cycle of X-PLOR refinement, both $|2F_o - F_c|$ and $|F_o - F_c|$ difference Fourier maps were calculated. These maps were then used to carry out manual fitting and rebuilding of the model. At later stages of refinement, water molecules were assigned when densities greater than 3σ were observed in the $|F_o| - |F_c|$ electron density map, which were within at least 3.3 Å of a potential hydrogen-bonding partner.

Acknowledgments

We thank Ming Wang for his expert assistance during data collection and phase analysis. This work was supported by USPHS grant #DK-42667 (to N. M. D. and J.-J. P. K.). This work was done during the tenure of an Established Investigatorship from the American Heart Association to N. M. D.

Received February 26, 1998; revised April 14, 1998.

References

Brünger, A.T. (1992). X-PLOR Version 3.1: A System for X-Ray Crystallography and NMR. (New Haven, CT: Yale University Press).

Carter, C., and Carter, C. (1979). Protein crystallization using incomplete factorial experiments. J. Biol. Chem. *246*, 12219–12223.

Dahms, N.M., and Brzycki-Wessell, M.A. (1995). Expression and characterization of functional bovine cation-dependent mannose 6-phosphate receptors in baculovirus-infected insect cells. Arch. Biochem. Biophys. *317*, 497–503.

Dahms, N.M., and Kornfeld, S. (1989). The cation-dependent mannose 6-phosphate receptor: structural requirements for mannose 6-phosphate binding and oligomerization. J. Biol. Chem. *264*, 11458–11467.

Dahms, N.M., Lobel, P., Breitmeyer, J., Chirgwin, J.M., and Kornfeld, S. (1987). 46 kDa mannose 6-phosphate receptor: cloning, expression, and homology to the 215 kDa mannose 6-phosphate receptor. Cell *50*, 181–192.

Dahms, N.M., Lobel, P., and Kornfeld, S. (1989). Mannose 6-phosphate receptors and lysosomal enzyme targeting. J. Biol. Chem. *264*, 12115–12118.

Dahms, N.M., Rose, P.A., Molkentin, J.D., Zhang, Y., and Brzycki, M.A. (1993). The bovine mannose 6-phosphate/insulin-like growth factor II receptor. The role of arginine residues in mannose 6-phosphate binding. J. Biol. Chem. *268*, 5457–5463.

Distler, J.J., Guo, J., Jourdian, G.W., Srivastava, O.P., and Hindsgaul, O. (1991). The binding specificity of high and low molecular weight phosphomannosyl receptors from bovine testes. Inhibition studies with chemically synthesized 6-O-phosphorylated oligomannosides. J. Biol. Chem. *266*, 21687–21692.

Drickamer, K. (1995). Multiplicity of lectin-carbohydrate interactions. Nat. Struct. Biol. *2*, 437–439.

Drickamer, K., and Taylor, M.E. (1993). Biology of animal lectins. Annu. Rev. Cell Biol. *9*, 237–264.

Furey, W., and Swaminathan, S. (1997). PHASES-95: a program package for the processing and analysis of diffraction data from macromolecules. In Macromolecular Crystallography Methods in Enzymology, C. Carter and R. Sweet, eds. (Orlando, FL: Academic Press).

Hoflack, B., and Kornfeld, S. (1985a). Lysosomal enzyme binding to mouse $P388D_1$ macrophage membranes lacking the 215-kDa mannose 6-phosphate receptor: evidence for the existence of a second mannose 6-phosphate receptor. Proc. Natl. Acad. Sci. USA *82*, 4428–4432.

Hoflack, B., and Kornfeld, S. (1985b). Purification and characterization of a cation-dependent mannose 6-phosphate receptor from murine P388D1 macrophages and bovine liver. J. Biol. Chem. *260*, 12008–12014.

Hoflack, B., Fujimoto, K., and Kornfeld, S. (1987). The interaction of phosphorylated oligosaccharides and lysosomal enzymes with bovine liver cation-dependent mannose 6-phosphate receptor. J. Biol. Chem. *262*, 123–129.

Holm, L., and Sander, C. (1993). Protein structure comparison by alignment of distance matrices. J. Mol. Biol. *233*, 123–138.

Jain, S., Drendel, W.B., Chen, Z.-W., Mathews, F.S., Sly, W.S., and Grubb, J.H. (1996). Structure of human β-glucuronidase reveals candidate lysosomal targeting and active-site motifs. Nat. Struct. Biol. *3*, 375–381.

Kornfeld, S. (1992). Structure and function of the mannose 6-phosphate/insulinlike growth factor II receptors. Annu. Rev. Biochem. *61*, 307–330.

Köster, A., Nagel, G., von Figura, K., and Pohlmann, R. (1991). Molecular cloning of the mouse 46-kDa mannose 6-phosphate receptor (MPR46). Biol. Chem. *372*, 297–300.

Li, M., Distler, J.J., and Jourdian, G.W. (1990). The aggregation and dissociation properties of a low molecular weight mannose 6-phosphate receptor from bovine testis. Arch. Biochem. Biophys. *283*, 150–157.

Livnah, O., Bayer, E.A., Wilchek, M., and Sussman, J.L. (1993). Three-dimensional structures of avidin and the avidin-biotin complex. Proc. Natl. Acad. Sci. USA *90*, 5076–5080.

Lobel, P., Dahms, N.M., and Kornfeld, S. (1988). Cloning and sequence analysis of the cation-independent mannose 6-phosphate receptor. J. Biol. Chem. *263*, 2563–2570.

Ma, Z., Grubb, J.H., and Sly, W.S. (1991). Cloning, sequencing, and functional characterization of the murine 46-kDa mannose 6-phosphate receptor. J. Biol. Chem. *266*, 10589–10595.

Ma, Z., Grubb, J.H., and Sly, W.S. (1992). Divalent cation-dependent stimulation of ligand binding to the 46-kDa mannose 6-phosphate receptor correlates with divalent cation-dependent tetramerization. J. Biol. Chem. *267*, 19017–19022.

Matthews, B.W. (1968). Solvent content of protein crystals. J. Mol. Biol. *3*, 491–497.

McPherson, A. (1982). Preparation and Analysis of Protein Crystals. (New York: Wiley).

Munier-Lehmann, H., Mauxion, F., and Hoflack, B. (1996a). Function of the two mannose 6-phosphate receptors in lysosomal enzyme transport. Biochem. Soc. Trans. *24*, 133–136.

Munier-Lehmann, H., Mauxion, F., Bauer, U., Lobel, P., and Hoflack, B. (1996b). Re-expression of the mannose 6-phosphate receptors in receptor-deficient fibroblasts. Complementary function of the two mannose 6-phosphate receptors in lysosomal enzyme targeting. J. Biol. Chem. *271*, 15166–15174.

Neufeld, E.F. (1991). Lysosomal storage diseases. Annu. Rev. Biochem. *60*, 257–280.

Otowinski, Z., and Minor, W. (1996). Processing of X-ray diffraction data collected in oscillation mode. Methods Enzymol. *276*, 307–326.

Punnonen, E.-L., Wilke, T., von Figura, K., and Hille-Rehfeld, A. (1996). The oligomeric state of 46-kDa mannose 6-phosphate receptor does not change upon intracellular recycling and binding of ligands. Eur. J. Biochem. *237*, 809–818.

Read, R.A. (1986). Improved coefficients for map calculation using partial structures with errors. Acta Crystallogr. *D5*, 760–763.

Roussel, A., and Cambillau, C. (1994). TURBO-FRODO, the Manual (Version 4.2). (Marseille, France: Biographics, LCCMB).

Shipley, J.M., Grubb, J.H., and Sly, W.S. (1993). The role of glycosylation and phosphorylation in the expression of active human β-glucuronidase. J. Biol. Chem. *268*, 12193–12198.

Sleat, D.E., and Lobel, P. (1997). Ligand binding specificities of the two mannose 6-phosphate receptors. J. Biol. Chem. *272*, 731–738.

Stein, M., Meyer, H.E., Hasilik, A., and von Figura, K. (1987). 46-kDa mannose 6-phosphate-specific receptor: purification, subunit composition, chemical modification. Biol. Chem. *368*, 927–936.

Terwilliger, T. (1994). HEAVY (Version 3.0) Manual. (Los Alamos, NM: Los Alamos National Laboratories).

Tong, P.Y., and Kornfeld, S. (1989). Ligand interactions of the cation-dependent mannose 6-phosphate receptor. Comparison with the cation-independent mannose 6-phosphate receptor. J. Biol. Chem. *264*, 7970–7975.

Tong, P.Y., Tollefsen, S.E., and Kornfeld, S. (1988). The cation-independent mannose 6-phosphate receptor binds insulin-like growth factor II. J. Biol. Chem. *263*, 2585–2588.

Tong, P.Y., Gregory, W., and Kornfeld, S. (1989). Ligand interactions of the cation-independent mannose 6-phosphate receptor. The stoichiometry of mannose 6-phosphate binding. J. Biol. Chem. *264*, 7962–7969.

von Figura, K., and Hasilik, A. (1986). Lysosomal enzymes and their receptors. Annu. Rev. Biochem. *55*, 167–193.

Waheed, A., Braulke, T., Junghans, U., and von Figura, K. (1988). Mannose 6-phosphate/insulin like growth factor II receptor: the two types of ligand bind simultaneously to one receptor at different sites. Biochem. Biophys. Res. Commun. *152*, 1248–1254.

Waheed, A., Hille, A., Junghans, U., and von Figura, K. (1990). Quaternary structure of the Mr 46,000 mannose 6-phosphate specific receptor: effect of ligand, pH, and receptor concentration on the equilibrium between dimeric and tetrameric receptor forms. Biochemistry *29*, 2449–2455.

Wang, B.C. (1985). Resolution of phase ambiguity in macromolecular crystallography. Methods Enzymol. *115*, 90–112.

Watanabe, H., Grubb, J.H., and Sly, W.S. (1990). The overexpressed human 46-kDa mannose 6-phosphate receptor mediates endocytosis and sorting of β-glucuronidase. Proc. Natl. Acad. Sci. USA *87*, 8036–8040.

Weis, W.I., and Drickamer, K. (1996). Structural basis of lectin-carbohydrate recognition. Annu. Rev. Biochem. *65*, 441–473.

Wendland, M., Hille, A., Nagel, G., Waheed, A., von Figura, K., and Pohlmann, R. (1989). Synthesis of a truncated Mr 46000 mannose 6-phosphate receptor that is secreted and retains ligand binding. Biochem. J. *260*, 201–206.

Wendland, M., Waheed, A., von Figura, K., and Pohlmann, R. (1991a). Mr 46,000 mannose 6-phosphate receptor. The role of histidine and arginine residues for binding of ligands. J. Biol. Chem. *266*, 2917–2923.

Wendland, M., von Figura, K., and Pohlmann, R. (1991b). Mutational analysis of disulfide bridges in the Mr 46,000 mannose 6-phosphate receptor. Localization and role for ligand binding. J. Biol. Chem. *266*, 7132–7136.

Westlund, B., Dahms, N.M., and Kornfeld, S. (1991). The bovine mannose 6-phosphate/insulin-like growth factor II receptor. Localization of mannose 6-phosphate binding sites to domains 1–3 and 7–11 of the extracytoplasmic region. J. Biol. Chem. *266*, 23233–23239.

Zhang, Y., and Dahms, N.M. (1993). Site-directed removal of N-glycosylation sites in the bovine cation-dependent mannose 6-phosphate receptor: effects on ligand binding, intracellular targeting and association with binding immunoglobulin protein. Biochem. J. *295*, 841–848.

Brookhaven Protein Data Bank Accession Number

The accession number for the coordinates of the structure reported in this paper is 1M6P.